

Two-particle correlations and the metal-insulator transition: Iterated Perturbation Theory revisited

Erik G. C. P. van Loon

Mathematical Physics Division, Department of Physics, Lund University, Lund, Sweden

Recent advances in many-body physics have made it possible to study correlated electron systems at the two-particle level. In Dynamical Mean-Field theory, it has been shown that the metal-insulator phase diagram is closely related to the eigenstructure of the susceptibility. So far, this situation has been studied using accurate but numerically expensive solvers. Here, the Iterated Perturbation Theory (IPT) approximation is used instead. Its simplicity makes it possible to obtain analytical results for the two-particle vertex and the DMFT Jacobian. The limited computational cost also enables a detailed comparison of analytical expressions for the response functions to results obtained using finite differences. At the same time, the approximate nature of IPT precludes an interpretation of the metal-insulator transition in terms of a Landau free energy functional.

Electronic correlations play an important role in a host of phase transitions, including unconventional superconductivity, charge-density waves and magnetism. However, the seminal example of a correlation induced transition is the Mott metal-insulator transition. Once the repulsive Coulomb interaction between electrons overpowers the band energy, the electrons localize and the density of states at the Fermi level disappears, turning the system into an insulator. The minimal theoretical description of this transition is given by the dynamical mean-field theory solution of the Hubbard model in the limit of infinite dimension [1].

In addition to the density of states, the metal-insulator transition also has profound effects on level of two-particle correlation functions. In equilibrium statistical physics, these carry three simultaneous meanings. First, as the probability for creating and annihilating fermions at four specific times. Secondly, as the second derivative of the free energy with respect to a particular field, indicating the energy cost or gain associated with fluctuations. Thirdly, as the linear response of a one-particle observable to an external field. In dynamical mean-field theory, these manifestations of two-particle correlations can be expressed entirely in terms of the local vertex [2–5].

Over the last few years, two-particle correlations close to the metal-insulator transition have been a topic of active investigations [5–8], partially driven by methodological and computational improvements that have enabled the accurate determination of the two-particle vertex [9–11]. Despite these improvements, the study of two-particle correlations typically requires a substantial amount of supercomputing power, because the evaluation of the two-particle vertex across a wide range of frequencies is hard.

This manuscript takes a step back and considers the Iterated Perturbation Theory approximation to dynamical mean-field theory. Within this approximation, the vertex can be evaluated analytically and this makes it possible to study two-particle correlations in detail and with a very limited computational cost.

I. DYNAMICAL MEAN-FIELD THEORY ON THE BETHE LATTICE

To set the stage, an overview of Dynamical Mean-Field Theory (DMFT) for the Hubbard on the Bethe lattice is given. More details can be found in the literature [1] and several aspects will be treated in more detail in subsequent sections.

A. Hubbard Model

The Hamiltonian of the Hubbard model is

$$H = -t \sum_{\langle ij \rangle} \sum_{\sigma=\uparrow,\downarrow} c_{i\sigma}^\dagger c_{j\sigma} + U \sum_i n_{i\uparrow} n_{i\downarrow}. \quad (1)$$

Here, $c_{i\sigma}^\dagger$ creates an electron with spin σ at site i , $c_{i\sigma}$ is the corresponding annihilation operator and $n = c^\dagger c$ is a number operator, $\langle ij \rangle$ denotes that the sum is taken only over pairs of neighboring sites. The physical parameters in the Hamiltonian are the electron hopping t and the electron-electron interaction U . Furthermore, the properties of the system depend on the temperature $T = 1/\beta$, the chemical potential (which determines the electron density) and the lattice. In this work, the Bethe lattice at half-filling is considered in the usual DMFT limit [1] of $z \rightarrow \infty$ with $t \propto 1/\sqrt{z}$, where z is the number of neighbors in the Bethe lattice. All calculations shown here use $t = 1/2$ for the rescaled hopping, leading to a bandwidth of 1 for the non-interacting system.

The model is known to undergo a metal-insulator phase transition as a function of U , at sufficiently low temperature $T \leq T_c$. At the critical temperature T_c , this transition is second-order and occurs at a critical interaction strength U_c . For the IPT approximation considered in this work, the critical point is known to occur at $U_c \approx 2.46$ and $T_c \approx 4.69 \cdot 10^{-2}$ [12], i.e. $\beta_c \approx 21.3$. Below T_c , there is a hysteresis region $U_{c1} \leq U \leq U_{c2}$ where both the metal and the insulator are stable solutions. Inside this region, there is also a third, thermodynamically unstable solution.

B. DMFT on the Bethe lattice

The three central objects in the theory are the (interacting) Green's function G , the bare Green's function G_0 and the self-energy Σ . All three objects are dynamical, in other words, they depend on the difference of two (imaginary) time coordinates or on a single (fermionic Matsubara) frequency. The relevance of these representations will be discussed in more detail in the following.

Dyson's equation provides the relation between these three objects in many-body theory,

$$G^{-1}(i\nu_n) = G_0^{-1}(i\nu_n) - \Sigma(i\nu_n), \quad (2)$$

where $i\nu_n$ denotes the n -th Matsubara frequency. This relation is evidently diagonal in the Matsubara representation. All three objects also depend on the spin, but paramagnetism is assumed in this manuscript and all spin labels are suppressed. Dyson's equation can be viewed as the definition of Σ .

In the formula above, all three objects are local. The lattice only enters the mean-field theory via the self-consistency condition. In the case of the Bethe lattice, the DMFT self-consistency condition is

$$G_0^{-1}(i\nu_n) = i\nu_n - t^2 G(i\nu_n). \quad (3)$$

This is the only place where the (scaled) hopping t enters the DMFT calculation. This relation is also diagonal in the Matsubara frequency.

It is sometimes useful to express this relation in terms of the so-called hybridization Δ ,

$$G_0^{-1}(i\nu_n) \equiv i\nu_n - \Delta(i\nu_n), \quad (4)$$

$$\Delta(i\nu_n) = t^2 G(i\nu_n). \quad (5)$$

This formulation of the self-consistency condition is a linear relation and it is therefore diagonal in other representations as well, as long as the representations are connected via linear transformations. For example, $\Delta(\tau) = t^2 G(\tau)$. This simple linear relationship between Δ and G is a peculiarity of the Bethe lattice.

The final ingredient for DMFT calculations is the solution of the many-body impurity problem defined by G_0 . The solution of this problem is done using a so-called impurity solver, which for the present discussion simply means an algorithm to calculate the functional relationship $\Sigma(G_0; U, \beta)$. This is the only place where U enters the DMFT calculation. In general, this functional is highly non-linear and non-local in time and couples all frequencies of the input G_0 and the output Σ . General results for two-particle properties of DMFT on the Bethe lattice will be derived below, which will contain the functional derivative $\partial\Sigma/\partial G_0$ or $\partial\Sigma/\partial\Delta$. Although this functional derivative is fundamentally accessible in, e.g., Quantum Monte Carlo solvers, it is a quantity that is expensive to calculate accurately. Iterated perturbation theory, introduced below in Sec. V, is an approximation with a particularly simple, explicit form for $\Sigma(G_0)$.

Thus, the derivative $\partial\Sigma^{\text{IPT}}/\partial G_0$ can be evaluated exactly at minimal cost.

In total, the DMFT self-consistency cycle consists of three relations $G_0 \xrightarrow{\text{impurity}} \Sigma \xrightarrow{\text{Dyson}} G \xrightarrow{\text{SC}} G_0$. The physical parameters U and t both only appear once in DMFT, in the self-energy and the self-consistency condition, respectively. The hopping t appears only as t^2 , i.e., the results are symmetric under the transformation $t \mapsto -t$, which is a manifestation of the particle-hole symmetry. The temperature does not appear explicitly. Instead, it determines the domains of the dynamical fields. In fact, with the Iterated Perturbation Theory impurity solver, all three DMFT+IPT relations are relatively simple to evaluate, with the only complication that basis transformations between imaginary time and Matsubara frequency are performed between some of the steps.

C. Dynamical fields: representations

The dynamical aspects of the Hubbard model are essential for the metal-insulator transition. Dyson's equation and the DMFT self-consistency condition are both diagonal in the Matsubara frequency. However, the Hubbard interaction U is instantaneous and thus couples different frequencies. In fact, the Iterated Perturbation Theory self-energy is essentially diagonal in imaginary time and the crux of DMFT+IPT lies entirely in the Fourier transforms between imaginary time and imaginary frequency. This makes it useful to explore in more detail the representations of the dynamical fields G , G_0 and Σ . In the imaginary time representation, the Green's function can be defined on the domain $[0, \beta)$, i.e., $G(\tau) : [0, \beta) \rightarrow \mathbb{R}$, where $\beta = 1/T$. The Green's function can then be extended to all τ via the relation $G(\tau - \beta) = -G(\tau)$. In other words, $G(\tau)$ is anti-periodic, reflecting the fermionic nature of the electron.

The Matsubara representation is obtained by performing a Fourier transformation,

$$G(i\nu_n) = \int_0^\beta d\tau G(\tau) \exp(+i\nu_n \tau) \quad (6)$$

$$G(\tau) = \frac{1}{\beta} \sum_{\nu_n} G(i\nu_n) \exp(-i\nu_n \tau), \quad (7)$$

where $\nu_n = (2n + 1)\pi T$ is the n -th Matsubara frequency. From the properties of $G(\tau)$, it follows that $G(-i\nu_n) = G(i\nu_n)^*$. In other words, $G(i\nu_n) : \mathbb{Z} \rightarrow \mathbb{C}$ can be restricted to $G(i\nu_n) : \mathbb{N} \rightarrow \mathbb{C}$ without losing any information. The Matsubara coefficients of the dynamical fields decay only algebraically as a function of n . Exact expressions for this decay can be derived, as discussed in Appendix A.

The imaginary time and Matsubara frequency representations both have a natural role in DMFT, since the Hubbard interaction is naturally written in imaginary time and Eqs. (2) and (3) are naturally written in the

Matsubara representation. However, both representations are not particularly *compact*. In imaginary time, a very fine discretization mesh is needed to faithfully describe the continuous function. As mentioned above, in the Matsubara representation, $G(i\nu_n)$ decays only algebraically and a large number of frequencies is needed to give a full description of the Green's function. The origin of this slow decay is the discontinuity of $G(\tau)$ and its derivatives at $\tau = 0$. Representing $G(\tau)$ in terms of appropriately chosen orthogonal basis sets turns out to be much more efficient [13]. Here, only the Legendre polynomials are considered, since these are already implemented in the TRIQS [14] computational framework. Following the notation of Ref. [13], the basis transformation is defined as

$$G(l) = \sqrt{2l+1} \int_0^\beta d\tau G(\tau) P_l(2\tau/\beta - 1), \quad (8)$$

$$G(\tau) = \sum_{l \geq 0} \frac{\sqrt{2l+1}}{\beta} G(l) P_l(2\tau/\beta - 1). \quad (9)$$

Since the Legendre polynomials P_l are real functions, $G(l)$ is real as well, so $G(l) : \mathbb{N} \rightarrow \mathbb{R}$.

The basis transformations to the Matsubara and Legendre representations are unitary and preserve the norm,

$$\|G\|^2 = \sum_{n=-\infty}^{\infty} |G(i\nu_n)|^2 = \beta \int_0^\beta |G(\tau)|^2 d\tau = \sum_l |G(l)|^2. \quad (10)$$

Altogether, the dynamical fields G , G_0 and Σ can be seen as vectors in an infinite-dimensional vector space. The various representations are simply providing different basis sets describing this vector space. On the other hand, not every element of these vector spaces is a valid, physical Green's function. The set of physical Green's functions can be considered as a manifold embedded in the relevant vector space. In some situations, further constraints apply, leading to a smaller subset of allowed Green's functions. An example is discussed in the next subsection.

D. Particle-hole symmetry

The Bethe lattice at half-filling is particle-hole symmetric and this leads to substantial simplifications in the analysis of DMFT. Particle-hole symmetry implies

$$\begin{aligned} G(\tau) &= G(\beta - \tau), \\ G(\tau) &= -G(-\tau), \\ \text{Re } G(i\nu_n) &= 0, \\ G(i\nu_n) &= -G(-i\nu_n), \\ G(l) &= 0 \text{ for } l \text{ odd.} \end{aligned}$$

Similar properties hold for the bare Green's function G_0 and the self-energy Σ , after removing the Hartree term in the latter.

For the Matsubara representation, this means that it is only necessary to consider the imaginary parts of the Green's function, so $G : \mathbb{N} \rightarrow \mathbb{R}, n \mapsto \text{Im } G(i\nu_n)$ is an element of the real vector space $\mathbb{R}^{\mathbb{N}}$.

II. FREE ENERGY FUNCTIONAL

Following Landau's theory of phase transitions, a free energy functional can be used to describe the hysteresis region of DMFT. For the Bethe lattice, this approach is described in detail in Section 3.7 of Ref. [4] and references therein [3, 15]. The lattice free energy functional can be written as $\Omega[\Delta] = \Omega^{\text{imp}} - \Omega'$, where Ω^{imp} is the free energy function of the impurity model, which satisfies $\frac{1}{T} \delta \Omega^{\text{imp}} / \delta \Delta(i\nu) = G(i\nu)$. The other term Ω' , the free energy associated with the lattice, has to ensure that the DMFT self-consistency condition is fulfilled at the extremal points of Ω . For the Bethe lattice, $\Omega' = \frac{T}{2t^2} \sum_{\nu} \Delta(i\nu)^2$ guarantees this, since $\frac{1}{T} \delta \Omega' / \delta \Delta(i\nu) = \Delta(i\nu)/t^2$, resulting in

$$0 = \frac{1}{T} \frac{\delta \Omega}{\delta \Delta(i\nu)} = G(i\nu) - \frac{\Delta(i\nu)}{t^2}, \quad (11)$$

which is the self-consistency condition of the Bethe lattice. The simple quadratic form of Ω' is a special property of the Bethe lattice and is very useful when considering higher-order derivatives, since all derivatives of Ω' beyond second-order vanish.

The second derivative of the free energy functional distinguishes stable (minimum) and unstable (maximum) solutions of the self-consistency equations. It is a matrix in Matsubara space,

$$\frac{1}{T} \frac{\delta^2 \Omega}{\delta \Delta(i\nu) \delta \Delta(i\nu')} = \frac{\delta G(i\nu)}{\delta \Delta(i\nu')} - \frac{\delta_{\nu\nu'}}{t^2} \quad (12)$$

$$= -G^2(i\nu) \frac{\delta G^{-1}(i\nu)}{\delta \Delta(i\nu')} - \frac{\delta_{\nu\nu'}}{t^2} \quad (13)$$

$$= G^2(i\nu) \left[\delta_{\nu\nu'} + \frac{\delta \Sigma(i\nu)}{\delta \Delta(i\nu')} \right] - \frac{\delta_{\nu\nu'}}{t^2} \quad (14)$$

$$= G^2(i\nu) [\delta_{\nu\nu'} + T F_{\nu\nu'} G^2(i\nu')] - \frac{\delta_{\nu\nu'}}{t^2}$$

$$\equiv \hat{\chi}_{\nu\nu'} - \frac{\delta_{\nu\nu'}}{t^2}. \quad (15)$$

Here, the reducible vertex F of the impurity model (following the notation in Ref. [5], $\omega = 0$ is implied everywhere),

$$\frac{\partial \Sigma(i\nu)}{\partial \Delta(i\nu')} \equiv \frac{1}{\beta} F_{\nu\nu'} G^2(i\nu'), \quad (16)$$

and the generalized susceptibility of the impurity model $\hat{\chi} = GG + GGF GG$ were introduced. The relation between $\hat{\chi}$ and F is a local Bethe-Salpeter equation. It should be pointed out that these equations are written

entirely in terms of the reducible vertex or the susceptibility of the impurity model. Since the impurity model at finite temperature cannot feature any phase transition, these objects are well-defined and divergence free. In particular, the inversion of a local Bethe-Salpeter to obtain the irreducible vertex is avoided in the present formulation.

In this Landau theory formulation, the Hessian $\delta^2\Omega/\delta\Delta^2$ is positive definite for stable solutions and has (at least) one negative eigenvalue for unstable solutions. At the critical point, one eigenvalue is exactly equal to zero, signalling the transition from a stable to an unstable solution. This also happens for the disappearing solution at the edge of the hysteresis region, where a stable and an unstable solution merge. The distinction between the critical point and the hysteresis region boundary can thus be found in the third derivative of the free energy: at the critical point $\delta^3\Omega/\delta\Delta^3 = 0$ along the “direction” given by the vanishing second derivative. For the Bethe lattice, $\delta^3\Omega/\delta\Delta^3 = \delta^3\Omega^{\text{imp}}/\delta\Delta^3$, since Ω' is quadratic in Δ .

III. DMFT ON THE BETHE LATTICE: ITERATIVE PROPERTIES

DMFT is a self-consistent theory, similar to Curie-Weiss mean-field theory for magnetism (see Appendix B for a brief overview). The difference is that Curie-Weiss theory considers a scalar as the self-consistently determined mean-field and DMFT uses a vector instead, the dynamical field. In both cases, forward iteration provides a way to achieve self-consistency. Starting from an initial guess G_0 , one calculates $G_0 \mapsto \Sigma \mapsto G \mapsto G_0$ until convergence is reached. Although only converged solutions have a formal role in the theory, useful physical insight can be gained by studying the convergence towards such a solution.

The convergence of forward iteration is determined by the DMFT Jacobian [4, 5, 12, 16]. The mathematical theory of self-consistent schemes states that the eigenvalues and eigenvectors of the Jacobian determine the iterative flow of the self-consistent scheme $\Delta^{(n+1)} = f(\Delta^{(n)})$. Starting with an initial guess $\Delta^{(0)}$ sufficiently close to a self-consistent solution Δ^* , the difference $\Delta^{(n)} - \Delta^*$ can be expanded in the eigenbasis of J . Every component then evolves as λ^n , where λ is the corresponding eigenvalue. In other words, the solution converges exponentially as long as all eigenvalues of J are smaller than unity in absolute value. Furthermore, smaller (absolute) eigenvalues lead to faster convergence.

Since the field in DMFT is an infinite-dimensional vector instead of the scalar in Curie-Weiss theory, the relevant Jacobian is an infinite-dimensional matrix. Note that the Jacobian keeps track of how a single object in the self-consistency cycle changes during the iterative process, so the expression for the Jacobian differs based on the object that is tracked, which will be illustrated by calculating the Jacobian for G_0 and for Δ . However,

these matrices are *similar*, they have the same eigenvalues, so the objects converge at the same speed, albeit with different frequency structures (eigenvectors).

A. Calculating the Jacobian

The Jacobian for G_0 is obtained by taking the derivative of the self-consistency condition,

$$J_{\nu\nu'}^{G_0} = \frac{\delta G_0^{\text{new}}(i\nu)}{\delta G_0^{\text{old}}(i\nu')} \quad (17)$$

$$= -G_0^2(i\nu) \frac{\delta(G_0^{-1})^{\text{new}}(i\nu)}{\delta G_0^{\text{old}}(i\nu')} \quad (18)$$

$$= t^2 G_0^2(i\nu) \frac{\delta G(i\nu)}{\delta G_0(i\nu')} \quad (19)$$

$$= t^2 G^2(i\nu) \left(\delta_{\nu\nu'} + G_0^2(i\nu) \frac{\delta\Sigma(i\nu)}{\delta G_0(i\nu')} \right). \quad (20)$$

Instead, it is also possible to calculate the Jacobian for the hybridization function Δ . The self-consistency condition for the hybridization function is $\Delta(i\nu) = t^2 G(i\nu)$, leading to

$$J_{\nu\nu'}^{\Delta} = \frac{\delta\Delta^{\text{new}}(i\nu)}{\delta\Delta^{\text{old}}(i\nu')} \quad (21)$$

$$= t^2 \frac{\delta G(i\nu)}{\delta\Delta(i\nu')} \quad (22)$$

$$= t^2 G^2(i\nu) \left(\delta_{\nu\nu'} + \frac{\delta\Sigma(i\nu)}{\delta\Delta(i\nu')} \right) \quad (23)$$

$$= t^2 G^2(i\nu) \left(\delta_{\nu\nu'} + \frac{\delta\Sigma(i\nu)}{\delta G_0(i\nu')} G_0^2(i\nu') \right). \quad (24)$$

This Jacobian is *similar* to the Jacobian for G_0 in Eq. (20), in the sense that they are related as $J^{\Delta} = P^{-1} J P$ for $P_{\nu\nu'} = \delta_{\nu\nu'} G_0^2(i\nu')$. Thus, they have the same eigenvalues and the forward iteration converges with the same speed, even though the eigenvectors are different.

It is useful to rewrite the results of (24) in terms of the vertex F , to get closer to the notation of Ref. [5]. In Sec. II, $F_{\nu\nu'}$ is defined as $T F_{\nu\nu'} G^2(i\nu') = \frac{\delta\Sigma(i\nu)}{\delta\Delta(i\nu')}$. This gives

$$J_{\nu\nu'}^{\Delta} = t^2 G^2(i\nu) \delta_{\nu\nu'} + t^2 T G^2(i\nu) F_{\nu\nu'} G^2(i\nu') = t^2 \hat{\chi}_{\nu\nu'}. \quad (25)$$

For some of the analysis, in particular the limiting cases discussed below, it is beneficial to split up the Jacobian into two terms, with and without a contribution from the vertex,

$$J_{\nu\nu'}^{\Delta} \equiv J_{\nu\nu'}^0 + J_{\nu\nu'}^1, \quad (26)$$

$$J_{\nu\nu'}^0 = t^2 G^2(i\nu) \delta_{\nu\nu'} \quad (27)$$

$$J_{\nu\nu'}^1 = t^2 T G^2(i\nu) F_{\nu\nu'} G^2(i\nu'). \quad (28)$$

The matrix $F_{\nu\nu'} = F_{\nu'\nu}$ is symmetric, so the Jacobian J^{Δ} is also symmetric. Generally, a function

$f(\Delta) : \mathbb{R}^N \rightarrow \mathbb{R}^N$ has a symmetric Jacobian if and only if [17] f is the derivative of some scalar function $g(\Delta) : \mathbb{R}^N \rightarrow \mathbb{R}$, $f_i = \partial g / \partial \Delta_i$. Here, this function g is actually known explicitly, since the right-hand side of the self-consistency condition for Δ , $t^2 G = t^2 \partial \Omega^{\text{imp}} / \partial \Delta$ is indeed the derivative of a scalar function. In fact, $J^\Delta = t^2 \partial^2 \Omega^{\text{imp}} / \partial \Delta^2 = t^2 \hat{\chi}$ follows immediately from a free-energy-based construction of DMFT combined with the Bethe lattice self-consistency condition. However, as will be discussed in Sec. VII and VIII, the derivation of the Jacobian from the self-consistency condition remains sensible even when the free-energy-based construction of DMFT fails.

B. Jacobian and lattice free energy

The relation between the Jacobian and the Hessian of the impurity free energy also provides a direct relation to the lattice free energy functional,

$$\frac{1}{T} \frac{\delta^2 \Omega}{\delta \Delta(i\nu) \delta \Delta(i\nu')} = \frac{1}{t^2} (J_{\nu\nu'}^\Delta - \delta_{\nu\nu'}). \quad (29)$$

Thus, the leading eigenvalue of the Jacobian, λ_J , is closely related to the metal-insulator phase diagram [4, 5, 12]. Above T_c , all eigenvalues of the Jacobian are smaller than unity in absolute value, i.e., $|\lambda_J| < 1$. The resulting solution is a minimum of the free energy functional [18]. Exactly at (U_c, T_c) , one eigenvalue is equal to unity. In the hysteresis region at $T < T_c$, the metallic and insulating solutions have eigenvalues smaller than unity, so they are stable. There is a third, unstable solution with eigenvalue larger than unity. At the boundary of the hysteresis region, the leading eigenvalues of the disappearing solutions (one stable and one unstable) are both equal to unity. Together, the leading eigenvalues of the possible solutions form a smooth curve, which implies an infinite slope of the disappearing solutions at the edge of the hysteresis region. This situation is illustrated in Fig. 12 of

Ref. [12].

As a side note, the DMFT self-consistency cycle also stops converging if $\lambda_J = -1$, even though this situation does not signal a special point in the free energy functional.

IV. RESPONSE FUNCTION: SELF-ENERGY VERSUS INTERACTION

The Jacobian also plays a role in the response of the observables of the system to changes in the model parameters. Simply stated, the DMFT response consists of the direct response of the impurity model combined with the self-consistent adjustment of the impurity model, which is described by the Jacobian. The first part is free from thermodynamic divergences by construction (at $T > 0$), whereas the second part can have non-smooth behavior when $\lambda_J = 1$. As an example, the compressibility has been studied in this way [5], although it remains smooth in the particle-hole symmetric model [5, 8, 19] because of the peculiar frequency structure of the leading eigenvector of the Jacobian. This motivates the study of a dynamic quantity, such as the self-energy Σ . Here, $d\Sigma/dU$ will be considered.

All three dynamical objects in the self-consistent procedure (G_0 , G and Σ) will vary when U is changed. The Dyson equation and Eq. (3) have to be satisfied at all values of U , thereby providing relations between the d/dU derivatives,

$$G^{-2} \frac{dG}{dU} = G_0^{-2} \frac{dG_0}{dU} + \frac{d\Sigma}{dU}, \quad (30)$$

$$\frac{dG_0}{dU} = G_0^2 t^2 \frac{dG}{dU}. \quad (31)$$

Note that these relations are all diagonal in the Matsubara representation and Matsubara frequencies are implied as the argument on all objects. Taken together, this gives $(1 - t^2 G^2) dG_0/dU = G_0^2 t^2 G^2 d\Sigma/dU$. This enables the calculation of the derivative of the self-energy as

$$\begin{aligned} \frac{d\Sigma^{\text{DMFT}}(i\nu_1)}{dU} &= \frac{\partial \Sigma^{\text{imp}}(i\nu_1)}{\partial U} + \sum_{\nu_2} \frac{\partial \Sigma^{\text{imp}}(i\nu_1)}{\partial G_0(i\nu_2)} \frac{dG_0(i\nu_2)}{dU} \\ &= \frac{\partial \Sigma^{\text{imp}}(i\nu_1)}{\partial U} + \sum_{\nu_2} \frac{\partial \Sigma^{\text{imp}}(i\nu_1)}{\partial G_0(i\nu_2)} \frac{t^2 G_0^2(i\nu_2) G^2(i\nu_2)}{1 - t^2 G^2(i\nu_2)} \frac{d\Sigma^{\text{DMFT}}(i\nu_2)}{dU} \\ \frac{d\Sigma^{\text{DMFT}}(i\nu_1)}{dU} &= \left(\frac{1}{1 - \frac{t^2 G_0^2 G^2}{1 - t^2 G^2} \frac{\partial \Sigma^{\text{imp}}}{\partial G_0}} \right)_{\nu_1 \nu_2} \frac{\partial \Sigma^{\text{imp}}(i\nu_2)}{\partial U} \end{aligned} \quad (32)$$

$$= \left(\frac{1 - t^2 G^2}{1 - t^2 G^2 - t^2 G_0^2 G^2 \frac{\partial \Sigma^{\text{imp}}}{\partial G_0}} \right)_{\nu_1 \nu_2} \frac{\partial \Sigma^{\text{imp}}(i\nu_2)}{\partial U} \quad (33)$$

At particle-hole symmetry, the numerator is diago-

nal and positive definite, since G is purely imaginary.

The denominator is of the form $\hat{1} - P^{-1}JG_0P$, where $P = G_0^2(i\nu)G^2(i\nu)\delta_{\nu\nu'}$. For stable solutions, the leading eigenvalue of the Jacobian J is smaller than unity, which implies that the matrix in the denominator has only positive eigenvalues. This property is preserved under a basis transformation to imaginary time [20], so $d\Sigma^{\text{DMFT}}(\tau)/dU = \int d\tau' M(\tau, \tau') d\Sigma^{\text{imp}}(\tau')/dU$ for some positive definite matrix M . The impurity model is a finite system and cannot feature phase transitions, so $d\Sigma^{\text{imp}}(\tau')/dU$ is finite. Thus, the denominator with the Jacobian is responsible for any non-smooth behavior of the self-energy as a function of U . This derivation provides a direct link between the iterative (in)stability and the behavior of the physically relevant object Σ as a function of the control parameter U .

V. ITERATED PERTURBATION THEORY

The missing ingredient in the discussion so far is the functional relation $\Sigma(G_0; U, \beta)$. In IPT, a particularly simple approximation for $\Sigma(G_0; U, \beta)$ is used, namely

$$\Sigma^{\text{IPT}}(\tau) = -U^2 G_0(\tau) G_0(-\tau) G_0(\tau). \quad (34)$$

This expression corresponds to applying second order as the impurity solver. The distinction between second-order perturbation theory and IPT is the way that the ‘‘input’’ G_0 is determined. In IPT, it is determined self-consistently according to the DMFT self-consistency condition. In second-order perturbation theory, on the other hand, it is either fixed to the initial G_0 or it is updated according to the Dyson equation in self-consistent SOPT. In the end, this difference is responsible for the fact that IPT has a metal-insulator transition and SOPT does not.

Note that this expression for the self-energy ignores the Hartree term, which is of first order in U and is instantaneous. When the density is fixed at half-filling, the Hartree term cancels with the chemical potential and there is no need to keep track of it explicitly.

A. Computational details

The TRIQS [14] package allows for easy manipulation of Green’s functions, including the Fourier transforms that are the essential part of the calculation. Here, a modified version of the IPT code available in TRIQS is used to perform calculations, it is available at [21]. In high-accuracy computations, it becomes necessary to enforce symmetry properties in the calculation explicitly, to avoid minor round-off errors from breaking symmetries. A single self-consistent DMFT+IPT calculation takes roughly a second on a normal desktop computer, without any parallelization, although very accurate calculations close to the phase transition can take somewhat longer. This low cost makes DMFT+IPT suitable for illustrating the Mott transition.

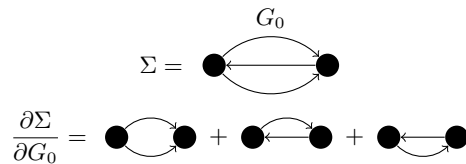


FIG. 1. Iterated Perturbation Theory self-energy and vertex

VI. THE IPT VERTEX

As discussed above, the derivative of the self-energy of the impurity model with respect to the input is needed for the stability analysis of DMFT, i.e., $\partial\Sigma/\partial G_0$ or $\partial\Sigma/\partial\Delta$ should be calculated. The relation between the two derivatives is

$$\frac{\partial\Sigma(i\nu)}{\partial\Delta(i\nu')} = \frac{\partial\Sigma(i\nu)}{\partial G_0(i\nu')} G_0^2(i\nu'). \quad (35)$$

In this manuscript, the name vertex is used for all three objects, F , $\partial\Sigma/\partial G_0$ and $\partial\Sigma/\partial\Delta$, the mathematical expression will be used when it is necessary to be specific. F is used in most of the DMFT literature, in IPT $\partial\Sigma/\partial G_0$ is actually easier to calculate. Their relation,

$$\frac{1}{\beta} F_{\nu\nu'} = \frac{\partial\Sigma(i\nu)}{\partial G_0(i\nu')} \frac{G_0^2(i\nu')}{G^2(i\nu')}, \quad (36)$$

has an important implication for the symmetry of these matrices. For an exact solution of the impurity model, F is a symmetric matrix, $F_{\nu\nu'} = F_{\nu'\nu}$, since it is related to the Hessian of the free energy. However, the IPT self-energy is given explicitly by Eq. (34) and it will turn out that the derivative $\partial\Sigma/\partial G_0$ is a symmetric matrix and that F is therefore not symmetric in IPT.

The defining equation of the IPT approximation is

$$\Sigma(\tau) = -U^2 G_0(\tau) G_0(-\tau) G_0(\tau). \quad (37)$$

The derivative $\partial\Sigma/\partial G_0$ can be taken directly, which will result in an expression that is quadratic in G_0 . The remainder of this section describes the mathematical properties of $\partial\Sigma/\partial G_0$ in detail, in both the imaginary time and Matsubara representation.

A. Imaginary time

At particle-hole symmetry, $G(-\tau) = -G(\tau)$ and the relation between Σ and G_0 is diagonal in the imaginary time representation,

$$\Sigma(\tau) = +U^2 G_0(\tau) G_0(\tau) G_0(\tau) \text{ at p.h.s.} \quad (38)$$

Note, in particular, that this relation can be inverted easily: given $\Sigma(\tau)$ and $U \neq 0$, $G_0(\tau)$ can be obtained uniquely as a third root. Thus, according to the inverse

function theorem, the derivative matrix $\partial\Sigma/\partial G_0$ is invertible, a property that necessarily holds in any representation.

Taking the derivative of the IPT self-energy gives

$$\frac{\partial\Sigma(\tau)}{\partial G_0(\tau')} = -2U^2 G_0(\tau)G_0(-\tau)\delta(\tau - \tau') \quad (39)$$

$$-U^2 G_0(\tau)^2 \delta(\tau + \tau'), \quad (40)$$

or, at particle-hole symmetry,

$$\left(\frac{\partial\Sigma(\tau)}{\partial G_0(\tau')}\right)^{\text{PHS}} = 3U^2 G_0^2(\tau)\delta(\tau - \tau'). \quad (41)$$

The latter result can be obtained directly from Eq. (38). It can also be derived from Eq. (40) by making the replacement $\partial G_0(\tau') \rightarrow \partial G_0(\tau') + \partial G_0(\beta - \tau')$, in other words, by taking the derivative within the particle-hole symmetric manifold.

Diagrammatically, taking a derivative corresponds to cutting a single line from every possible self-energy diagram in every possible way, see Fig. 1. The IPT self-energy functional consists of a single diagram with three internal lines G_0 , so there are three possible ways to cut a line. This explains the prefactor 3. The difference between $\partial/\partial G_0$ and $\partial/\partial\Delta$ is the precise way the cutting of the line is handled: in $\partial/\partial G_0$ the ‘‘stumps’’ left by the cut are amputated with G_0 , whereas in $\partial/\partial\Delta$ a factor G_0 is attached at the stumps. Finally, in the definition of F , the ends of the $\partial/\partial\Delta$ expression are divided by G . In total, the definition of F amputates not only G_0 but also the one-particle irreducible part of the legs. In the exact solution, these are generated by higher orders in U , but in IPT these one-particle irreducible parts are absent completely. In IPT, the definition of F amputates too much.

The derivative, $\frac{\partial\Sigma(\tau)}{\partial G_0(\tau')}$, interpreted as a matrix in imaginary time, is diagonal with strictly positive elements on the diagonal. The operator is therefore positive definite if $U \neq 0$, which is a property that is independent of the choice of basis, i.e., it also holds in the Matsubara basis. The matrix also has a well-defined inverse (again, if $U \neq 0$), which was already guaranteed by the inverse function theorem. As a diagonal matrix, $\frac{\partial\Sigma(\tau)}{\partial G_0(\tau')}$ is also symmetric. This is actually an undesirable property of IPT, since it implies that $F_{\nu\nu'}$ is not symmetric with the IPT approximation.

B. Matsubara representation

It is also useful to express the self-energy and the functional derivative in the Matsubara representation. This can be done diagrammatically, or by Fourier transforming the previously obtained imaginary time expressions,

see also Appendix C. Either way,

$$\Sigma(i\nu) = -\frac{U^2}{\beta^2} \sum_{\nu_1\nu_2} G_0(i\nu_1)G_0(i\nu_2)G_0(i\nu_1 + i\nu_2 - i\nu), \quad (42)$$

leading to

$$\begin{aligned} \frac{\delta\Sigma(i\nu)}{\delta G_0(i\nu')} &= -2\frac{U^2}{\beta^2} \sum_{\nu_1} G_0(i\nu_1)G_0(i\nu_1 + i\nu' - i\nu) \\ &\quad - \frac{U^2}{\beta^2} \sum_{\nu_1} G_0(i\nu_1)G_0(i\nu + i\nu' - i\nu_1) \end{aligned} \quad (43)$$

The functional derivative $\delta\Sigma(i\nu)/\delta G_0(i\nu')$ is a matrix in ν, ν' . Since there is a relation between the value of the Green’s function at positive and negative Matsubara frequencies, it is generally sufficient to consider the symmetric and antisymmetric parts of the matrix separately [22]. The functional derivative $\partial\Sigma(i\nu)/\partial G_0(i\nu')$ shows how much the self-energy at Matsubara frequency ν changes when the input G_0 at frequency ν' is varied. At particle-hole symmetry, only the functional derivative within the particle-hole symmetric manifold ($G_0(i\nu) = -G_0(-i\nu)$) is needed [23]. This restricts variations to the form

$$\delta G_0(|\nu|) \equiv \delta G_0(i\nu) - \delta G_0(-i\nu). \quad (44)$$

The associated functional derivative $\delta\Sigma(\nu)/\delta G(|\nu'|)$ is

$$\begin{aligned} \delta\Sigma(\nu)/\delta G_0(|\nu'|) &= -3\frac{U^2}{\beta^2} \sum_{\nu_i} [G_0(i\nu_i)G_0(i\nu_i + i\nu' - i\nu) \\ &\quad - G_0(i\nu_i)G_0(i\nu_i - i\nu' - i\nu)]. \end{aligned} \quad (45)$$

This result can be obtained from the previous result by explicitly using Eq. (44). A more compact expression is obtained by defining a ‘‘bare susceptibility’’ χ as

$$\begin{aligned} \chi(i\omega) &= -\sum_{\nu_1} G_0(i\nu_1)G_0(i\nu_1 - i\omega), \quad (46) \\ \delta\Sigma(\nu)/\delta G_0(|\nu'|) &= 3\frac{U^2}{\beta^2} [\chi(i\nu - i\nu') - \chi(i\nu + i\nu')]. \end{aligned}$$

Differences and sums of fermionic Matsubara frequencies appear here, which results in bosonic Matsubara frequencies, e.g., $\nu_i - \nu_j = (2i - 2j)\pi T = \omega_{i-j}$ and $\nu_i + \nu_j = (2i + 2j + 2)\pi T = \omega_{i+j+1}$. An important detail is the +1 in the last expression. Note that χ is real and positive, since G_0 is purely imaginary.

It is easy to verify that $\chi(-i\omega) = \chi(i\omega)$, by relabelling $\nu_1 \rightarrow \nu_2 = \nu_1 - \omega$, so the expression for $\partial\Sigma(i\nu)/\partial G_0(|\nu'|)$ is properly antisymmetric in ν . This confirms that Σ remains particle-hole symmetric as long as G_0 is particle-hole symmetric. Of course, that can also be seen immediately in the imaginary time representation.

The frequency structure of the vertex is given entirely by $\chi(i\nu - i\nu') - \chi(i\nu + i\nu')$, with $3U^2/\beta^2$ appearing as

a simple prefactor. At particle-hole symmetry, it is sufficient to consider the matrix $\delta\Sigma(i\nu)/\delta G_0(|\nu'|)$ for $\nu > 0$ and $\nu' > 0$. This matrix is real and symmetric. The first contribution, $\chi(i\nu - i\nu')$, depends only on the distance to the diagonal of the matrix (Toeplitz matrix), whereas the second contribution, $\chi(i\nu + i\nu')$ depends only on the Manhattan distance to the top-left corner of the matrix (Hankel matrix), see Fig. 2. Note that that Hartree term in the self-energy would provide a term proportional to U^1 in the vertex, but this term would be symmetric in the fermionic frequency and at particle-hole symmetry only the frequency-antisymmetric part plays a (non-trivial) role.

Furthermore, it is interesting to point out that $\chi(\omega_0) = \|G_0\|^2$ according [24] to Eq. (10). In fact, this expression can be generalised to an expression for $\chi(\omega_n)$,

$$\chi(\omega_n) = \int_0^\beta d\tau \cos(\omega_n \tau) G^2(\tau), \quad (47)$$

where symmetry was used to obtain the cos instead of a complex exponential. Since $G^2(\tau)$ is positive-definite and $\cos(\omega_n \tau) \leq 1$, this implies that $0 \leq \chi(\omega_n) \leq \chi(\omega_0)$. Although no mathematical proof is given here [25], numerically it turns out that $\chi(\omega_n)$ is a decreasing function of $n \geq 0$. This implies that all matrix elements are positive, since they are of the form $\chi(\omega_a) - \chi(\omega_b)$ with $b > a \geq 0$. A notable exception is the atomic limit [26], discussed below, where $\chi(\omega_n) = 0$ for $n > 0$. A further remark is that $G_0(\tau) \rightarrow \chi(\tau) = G_0(\tau)G_0(\tau)$ can be inverted trivially, since the sign of $G_0(\tau)$ is fixed, so the mapping between G_0 and the vertex is one-to-one, given fixed values of U and β .

The relative magnitude of the matrix elements might be of use when estimating the magnitude of eigenvalues of the vertex, since the Gershgorin circle theorem [27] needs the sum of absolute values of rows/columns of the matrix $\chi(i\nu - i\nu') - \chi(i\nu + i\nu')$, which are simply given by $R_j = \chi(i\omega_0) + 2 \sum_{m=1}^j \chi(i\omega_m)$ here. For the vertex, the prefactor $3U^2/\beta^2$ does not change the eigenstructure. It is plausible that further analytical results can be derived for the IPT vertex given suitable assumptions on G_0 .

The IPT results for the vertex are very simple compared to what one would find using exact diagonalization or quantum Monte Carlo, since it is given by a very small number of diagrams (only one diagram is sufficient at particle-hole symmetry). It is not necessary to resort to channel decomposition techniques [28, 29], since this decomposition in terms of a ‘‘susceptibility’’ occurs naturally. Unlike the usual channel decompositions, the ‘‘susceptibility’’ that appears here is based on $G_0 G_0$ and not on GG .

C. Higher-order vertices

Having determined the vertex $\partial\Sigma/\partial G_0$, it is also possible to consider higher-order derivatives. In IPT,

$$\frac{\beta^2}{3U^2} \frac{\partial\Sigma}{\partial G_0}$$

$\chi(i\nu - i\nu')$

χ(ω ₀)	χ(ω ₁)	χ(ω ₂)
χ(ω ₁)	χ(ω ₀)	χ(ω ₁)
χ(ω ₂)	χ(ω ₁)	χ(ω ₀)

−

$\chi(i\nu + i\nu')$

χ(ω ₁)	χ(ω ₂)	χ(ω ₃)
χ(ω ₂)	χ(ω ₃)	χ(ω ₄)
χ(ω ₃)	χ(ω ₄)	χ(ω ₅)

FIG. 2. The IPT vertex is given by the difference between a Toeplitz matrix (left) and a Hankel matrix (right), and a prefactor $3U^2/\beta^2$.

$\partial^2\Sigma/\partial G_0^2$ and $\partial^3\Sigma/\partial G_0^3$ are finite, and all higher orders are equal to zero. This follows from the explicit IPT form of the self-energy and is a notable difference with the exact solution.

VII. FAILURE OF THE FREE ENERGY FUNCTIONAL IN IPT

The derivation of the free energy functional in Sec. II holds for the general formulation of DMFT. However, a problem is encountered when IPT is used as the impurity solver. As discussed above, $F_{\nu\nu'}$ is not a symmetric matrix in IPT, which would imply that the Hessian of the free energy functional is not symmetric, which is impossible. Thus, the conclusion is that there is no consistent way to derive IPT from a free energy functional. However, the Jacobian is still useful to characterize the hysteresis region, as will be discussed in Sec. VIII.

The lack of a free energy functional might come as a surprise. It is useful to consider an analogy in the form of electromagnetism. In electrostatics, the electric field \vec{E} is curl-free, $\nabla \times \vec{E} = 0$, i.e., the matrix $\partial E_i/\partial x_j$ is symmetric. This property guarantees that the electric field can be written as the gradient of a potential V , $\vec{E} = -\nabla V$. Given \vec{E} , $V(\vec{x})$ can be determined up to a constant by simply taking a line integral of \vec{E} from any point \vec{x}_0 . Due to the vanishing curl, this construction is independent of the integration path. Now, imagine that we had an approximate way to calculate the electric field for a system of interest, $\vec{E}^{\text{approx}}(\vec{x})$. If this approximation satisfies $\nabla \times \vec{E}^{\text{approx}} = 0$, then there is still a consistent way to construct V^{approx} via line integrals. However, if $\nabla \times \vec{E}^{\text{approx}} \neq 0$, the construction breaks down. \vec{E}^{approx} can still be a useful approximation for the electric field, it just does not allow a discussion of potentials. The situation is similar in IPT, in the sense that the explicit recipe $G^{\text{SOPT}}(\Delta)$ of the IPT impurity solver is inconsistent with

the existence of a free energy functional $\Omega^{\text{imp}}[\Delta]$ with $G^{\text{SOPT}} = T^{-1}\partial\Omega^{\text{imp}}/\partial\Delta$.

VIII. JACOBIAN IN IPT

The two-particle vertex appears in the general expression for the DMFT Jacobian. Having derived the IPT vertex, it is now possible to study the IPT Jacobian matrix (not just the leading eigenvalue) in more detail. Below, the Jacobian is evaluated analytically in several limiting cases, namely in the non-interacting ($U = 0$) and in the atomic ($t = 0$) limit, as well as in the limit of large frequency. In these simple situations, the Jacobian is diagonal in the Matsubara frequency. Additional $T = 0$ expressions are given in Appendix D. However, some consideration of the structure of the Jacobian is necessary first.

1. Jacobian as a symmetric matrix

The Jacobian for DMFT is given in Equation (20). For an exact solution of the impurity model, F is a symmetric matrix and J^Δ is thus also symmetric. However, within the IPT approximation, J^Δ is not symmetric, it is only *similar* to a symmetric matrix: defining $X_{\nu\nu'} = \delta_{\nu\nu'}G(i\nu)/G_0(i\nu)$, the matrix $X^{-1}J^\Delta X$ is real and symmetric. Essentially, one factor $G(i\nu)/G_0(i\nu)$ is divided out from the left in Eq. (24) and replaced by a factor $G(i\nu')/G_0(i\nu')$ from the right. Due to the similarity, the non-symmetric J^Δ still has real eigenvalues and the symmetrized version of J has an orthogonal basis of eigenvectors. The factors (G/G_0) are related to the amputation procedure of the vertex.

2. Non-interacting model

The DMFT self-consistency cycle becomes trivial in the non-interacting model, $U = 0$, since it implies $\Sigma = 0$, $G_0 = G$ and the self-consistency condition becomes $G^{-1}(i\nu_n) = i\nu_n - t^2G(i\nu_n)$, which is solved by $G(i\nu) = \frac{i\nu - \sqrt{(i\nu)^2 - 4t^2}}{2t^2}$.

Since there is no self-energy at $U = 0$, the Jacobian is given by the first, diagonal term, i.e., $J_{\nu\nu'} = J_{\nu\nu'}^0 = t^2G_r^2\delta_{\nu\nu'}$. In other words, the generalized susceptibility is given by the bubble diagram. The eigenvectors consist of a single positive Matsubara frequency and the eigenvalues are simply $-t^2|G(i\nu_n)|^2 < 0$. For the solution given above, $-t^2|G(i\nu_n)|^2 > -1$ for $\nu_n > 0$. So for $T > 0$, this solution is iteratively stable, although it becomes unstable at $T = 0$. The leading eigenvector is entirely localized on the lowest Matsubara frequency.

This result was derived without using the IPT approximation explicitly, since the result $\Sigma = 0$ is exact at $U = 0$.

Thus, the Jacobian at $U = 0$ depends only on the temperature and the lattice, as one should expect.

3. Atomic limit

In the atomic limit, $t = 0$, the self-consistency condition is $G_0 = 1/i\nu_n$ and this makes it possible to evaluate χ explicitly,

$$\chi(\omega_0) = \frac{1}{\pi^2 T^2} \sum_n \frac{1}{2n+1} \frac{1}{2n+1} = \frac{1}{4T^2}. \quad (48)$$

For finite frequency $a \neq 0$, manipulations similar to the usual evaluation of the Lindhard bubble give

$$\begin{aligned} G_0(i\nu_n)G_0(i\nu_{n+a}) &= \frac{G_0(i\nu_n) - G_0(i\nu_{n+a})}{G_0^{-1}(i\nu_{n+a}) - G_0^{-1}(i\nu_n)} \\ &= \frac{G_0(i\nu_n) - G_0(i\nu_{n+a})}{2ai}, \\ \chi(\omega_a) &= \sum_n G_0(i\nu_n)G_0(i\nu_{n+a}) \\ &= \frac{1}{2ai} \left(\sum_n G_0(i\nu_n) - \sum_n G_0(i\nu_{n+a}) \right) \\ &= 0. \end{aligned} \quad (49)$$

This reflects the fact that the atomic limit does not have any charge dynamics. Looking at Eq. (45) or at Fig. 2, the vertex is proportional to the identity matrix [30].

At $t = 0$, the Jacobian is strictly equal to zero. However, for $0 < t \ll U$, the atomic G_0 and vertex can still be used, while the Jacobian is given only by J^Σ and is diagonal. Due to the factors G^2 and G_0^2 , it is decaying as a function of frequency. Importantly, it results in $J > 0$ in the atomic limit, since $G^2G_0^2$ is positive. Together with the non-interacting result, this shows that all eigenvalues of the Jacobian have to change sign somewhere between $U = 0$ and $U \gg t$.

4. Large frequency

Simplifications are also possible in the limit of large frequency, i.e., $\nu, \nu' \ll t, U$. Looking at the vertex in Fig. 2, since $\chi(i\omega_n)$ is a decreasing function of the frequency, only the Toeplitz matrix survives in the limit of large frequency. It depends only on $\nu - \nu'$ and is bounded by $\chi(\omega_0)$. In the Jacobian, the contribution coming from the vertex has to be compared against the $\delta_{\nu\nu'}$ term. The vertex contribution contains an additional prefactor $G_0(i\nu)^2$, which decays at large frequency. Thus, the Jacobian becomes dominated by the diagonal contribution, $J \approx J^0 = t^2G^2(i\nu)\delta_{\nu\nu'}$ at large frequency. The resulting eigenvalues are simply $t^2G^2(i\nu_n) < 0$ and decay asymptotically as $-t^2\nu_n^{-2}$. In other words, as long as U and t are finite, the spectrum of the Jacobian contains a countably infinite number of eigenvalues that approaches 0 from below.

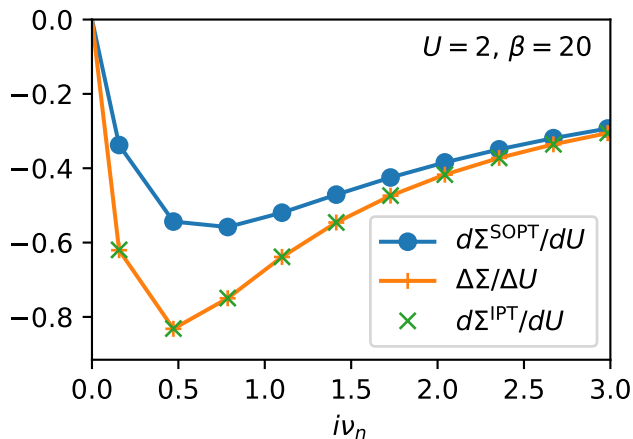


FIG. 3. $d\Sigma/dU$ evaluated analytical via Eq. (33) and numerical via the finite difference $\Delta U = 0.001$. The IPT response is enhanced compared to the SOPT response (where G_0 is held constant) due to the self-consistent feedback.

IX. RESPONSE IN IPT

In Eq. (33), the derivative of the DMFT self-energy with respect to the interaction was expressed in terms of impurity properties. The vector $d\Sigma^{\text{DMFT}}/dU$ could generally be written as a positive definite matrix (for stable solutions) times the vector $d\Sigma^{\text{imp}}/dU$. For iterated perturbation theory, $\Sigma^{\text{imp}} = \Sigma^{\text{SOPT}}$, and $\partial\Sigma^{\text{SOPT}}(\tau')/\partial U = 2UG_0(\tau')^3$ is sign definite (negative). This then implies $d\Sigma^{\text{IPT}}(\tau)/dU < 0$ for $U > 0$. Using the fact that Σ depends only on U^2 , this statement can be reformulated as $d\Sigma^{\text{IPT}}(\tau)/d(U^2) < 0$, for all $\tau \in [0, \beta)$. Note also that, since $\Sigma(\tau) < 0$, there is the implication $d\|\Sigma\|^2/d(U^2) > 0$, which is representation independent.

This proof of monotonicity only holds for stable solutions, $\lambda_J < 1$, in other words, it does not apply to the disappearing solutions at the edge of the hysteresis region or at the critical point, where $\lambda_J = 1$ and $\partial_U \Sigma$ is divergent, nor to the third, thermodynamically unstable solution that exists within the hysteresis region with $\lambda_J > 1$. Exactly at the critical point, $\lambda_J = 1$ and the self-energy has infinite slope.

A numerical illustration of Eq. (33) is given in Fig. 3.

X. JACOBIAN IN THE METAL AND THE INSULATOR

Moving beyond analytical results in limiting cases, numerical calculations can be done at arbitrary U and T . Figure 4 shows the results of a calculation at $U = 1.5$ and $\beta = 35$, in the metallic regime. The blue lines in Fig. 4 show G_0 , Σ and G , respectively. The metallicity is visible in the linearly vanishing Σ around $\nu_n = 0$.

The orange lines in Fig. 4(a) show the normalized difference vector between subsequent iterations. The differ-

ence vectors are eigenvectors of the respective Jacobians. There is a clear difference in frequency structure between the difference vectors of G_0 and G on the one hand and Σ on the other hand. The latter features a continuous decay with a uniform sign. The former has a sign change between the lowest Matsubara frequency and the higher Matsubara frequencies. Although the Jacobians are *similar* and have the same eigenvalues, they are not identical and have different eigenvectors. Thus, the change of basis matrices connecting the Jacobians are responsible for the varying shapes of the difference vectors.

Figure 4(b) shows the convergence towards the self-consistent solution. After a few iterations, all frequencies are exponentially converging with a single exponent, showing that there is a single relevant eigenvalue of the Jacobian and that the corresponding eigenvector is finite at all Matsubara frequencies. Here, $\delta\Sigma$ is the change in $\text{Im} \Sigma$ between subsequent iterations. The magnitude of the change becomes smaller for larger Matsubara frequencies. In fact, $\delta\Sigma(i\nu)$ decays as ν^{-3} at large frequencies, since only odd powers in the asymptotic expansion are allowed at particle-hole symmetry, and the ν^{-1} coefficient of Σ is fixed by the parameter U , see Appendix A. The simplicity of IPT makes it possible to track the convergence with high accuracy, as is clear from the values of the y-axis.

Finally, Fig. 4(c) shows the eigenvalues of the Jacobian evaluated according to Eq. (20) in blue, with the orange line giving the scaling obtained directly from the iterations in Fig. 4(b). This confirms that the largest absolute eigenvalue determines the convergence. As in the limit $U = 0$, the eigenvalues are negative. The second eigenvalue is already almost half as small as the leading eigenvalue.

Moving to the insulating side of the phase diagram, Fig 5 shows results at $U = 3$. The self-energy is insulating, as is visible in Fig 5(a). Once again, exponential convergence occurs at all frequencies, with the difference vector rapidly decaying as a function of frequency. At the same time, several qualitative changes have occurred. First of all, the leading eigenvalues of the Jacobian have changed sign, as anticipated by the results for the atomic limit. Secondly, the shape of the difference vectors has changed substantially. Now, the difference vectors for the self-energy Σ and G_0 are very similar, whereas the one of G differs. Furthermore, a sign change within the difference vector no longer occurs. The difference vectors for G_0 and Σ are almost entirely localized on the lowest Matsubara frequency, as would be expected close to the atomic limit (see Sec. VIII 3). Away from the two limits, the off-diagonal parts of the vertex are not zero, so the eigenvectors of the Jacobian consist of more than a single Matsubara frequency.

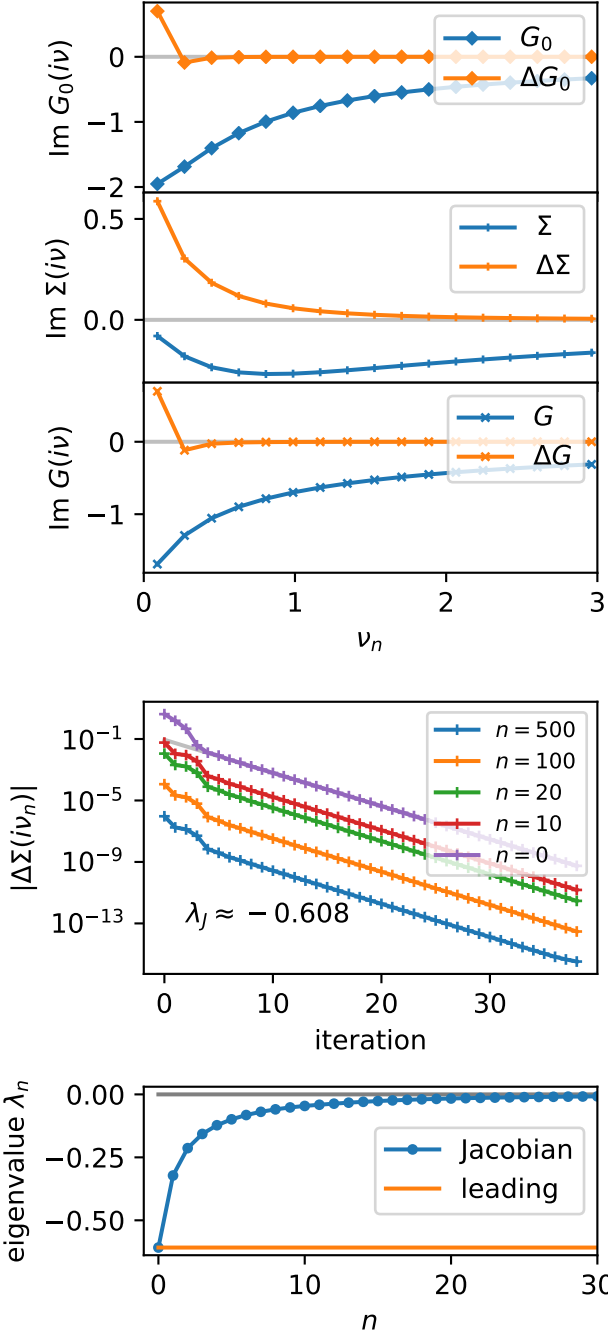


FIG. 4. Calculations at $U = 1.5$, $\beta = 35$. (a) converged solution (blue) and normalized difference vector (orange). (b) the self-energy converges exponentially in the forward iteration, $\Delta \Sigma(i\nu_n) \propto J^{\text{iteration}}$ at all frequencies, with the same exponent. (c) The first eigenvalues of the Jacobian, sorted by their absolute value. The value of λ_J found in (b) corresponds to the leading eigenvalue here.

XI. CLOSE TO THE CRITICAL POINT

Ref. [12] puts the critical point at $U_c \approx 2.46$ and $\beta_c \approx 21.3$ in units of $t = 1/2$. To illustrate the approach to

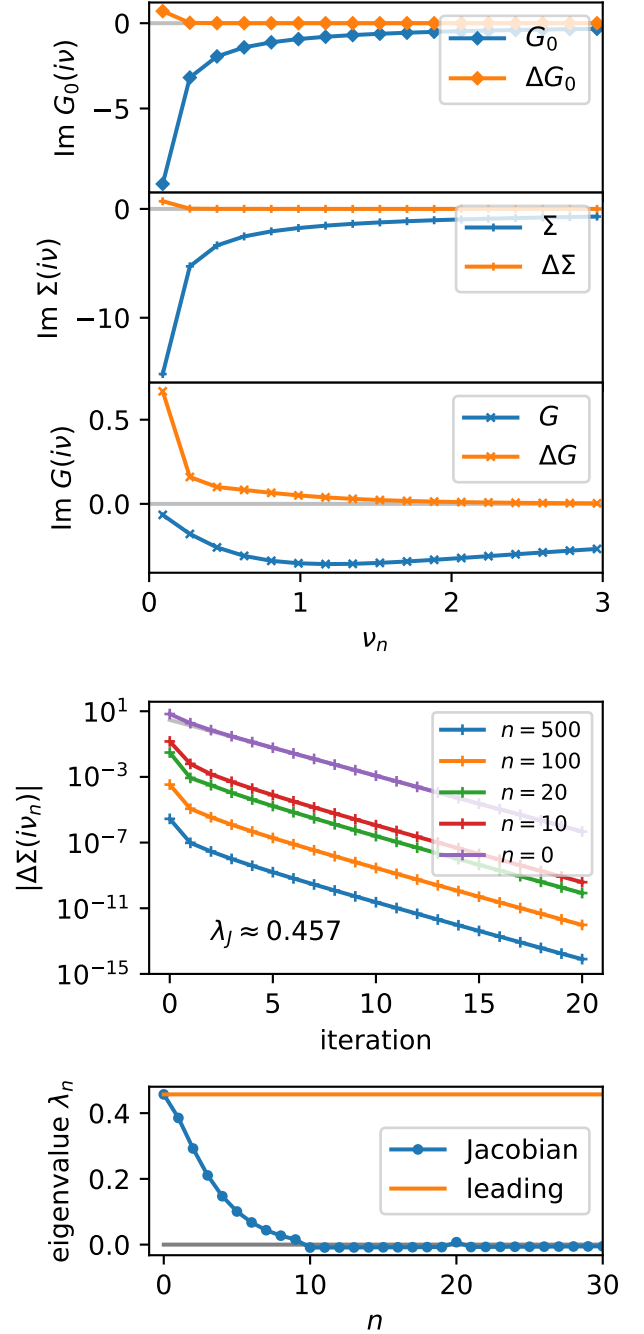


FIG. 5. Calculations at $U = 3$, $\beta = 35$, see also Fig 4.

the critical point, Fig. 6 shows a scan over U at $\beta = 20$, i.e., for $T > T_c$. Every simulation is started from the solution at $U = U - \Delta U$, with $\Delta U = 0.01$, starting from the initial solution at $U = 0$. A convergence goal of 10^{-8} for the $G_0(i\nu_n)$ in subsequent iterations is used, which is reached in a few hundred iterations close to U_c .

The leading eigenvalue starts out negative, as expected for the non-interacting limit. This continues until $U \approx 1.9$, where a positive eigenvalue takes over, since J^Σ becomes more important than J^0 . This happens clearly

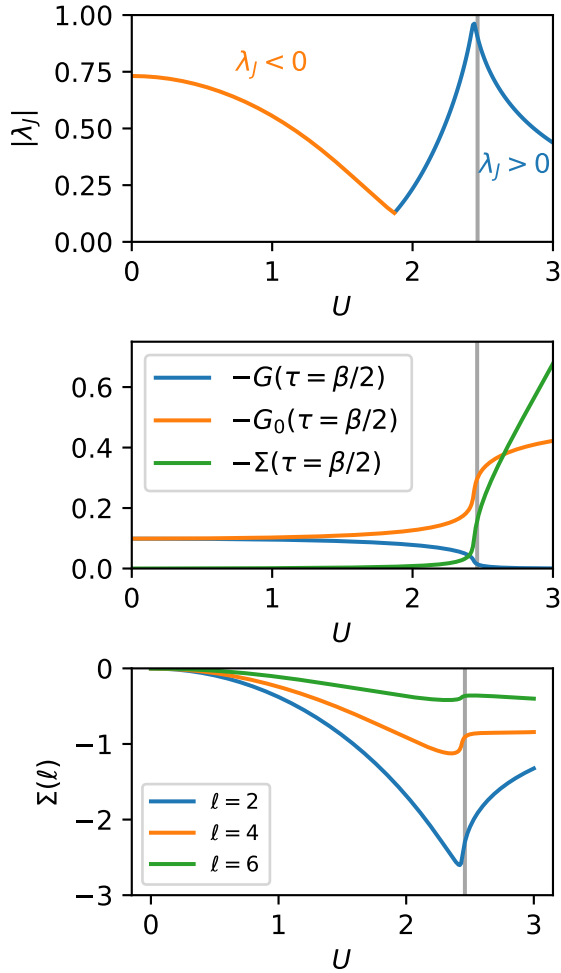


FIG. 6. Results at $\beta = 20$, which is just above the hysteresis region. (a) The leading eigenvalue $|\lambda_J|$ reaches a maximum just below unity close to U_c (gray line, value from Ref. [12]). The blue curve denotes that the leading eigenvalue is positive, as in the atomic limit, the orange curve that the leading eigenvalue is negative, as in the non-interacting limit. (b) The imaginary-time Green's functions and self-energy evaluated at $\tau = \beta/2$. They change rapidly in the region where $\lambda_J \approx +1$. (c) The evolution of Σ in the Legendre basis shows that not all properties are monotonous functions of U .

before U_c , since the eigenvalue is far below unity. Close to U_c , the leading eigenvalue comes close to unity, but does not quite reach it since $T > T_c$ here. Afterwards, the leading eigenvalue decays quickly.

Quantities of physical interest, such as $G(\tau = \beta/2)$, $G_0(\tau = \beta/2)$ and $\Sigma(\tau = \beta/2)$, change rapidly in the region where $\lambda_J \approx 1$. As proven in Sec. 33, $\Sigma(\tau)$ depends monotonously on U . $G_0(\tau = \beta/2)$ and $G(\tau = \beta/2)$ also appear to be monotonous in U , although the formal proof only holds for Σ . However, Fig. 6(c) clearly shows that not all quantities are monotonous in U : the Legendre coefficients of the self-energy have a minimum at intermediate U .

Fig. 7(a) shows the Matsubara Green's function for

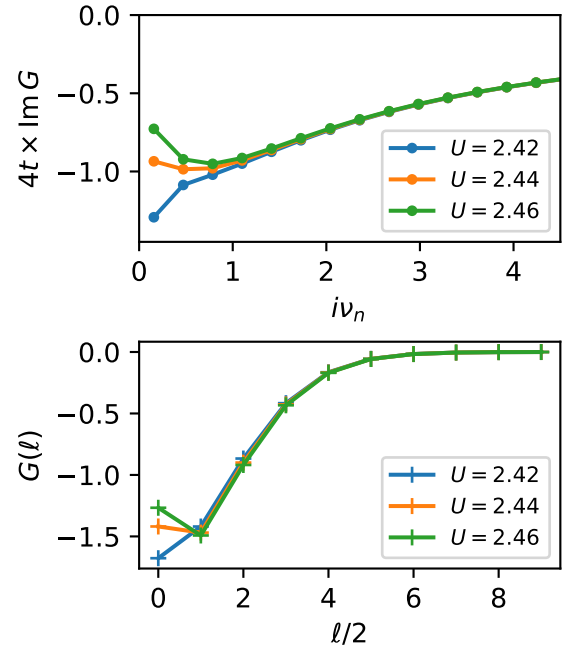


FIG. 7. The Green's function in the Matsubara and Legendre representation at $T = 1/20$, just above T_c and close to U_c . The shape of the curves at low frequency changes rapidly with U .

several value of U close to the critical point. The temperature is $T = 1/20 > T_c$, as in Fig. 6. The Green's function has been rescaled by $4t$ here, showing that $G(i\nu_0) \approx G(i\nu_1) \approx 1/(4t)$. It is directly visible that the slope of G changes as a function of U , which is a reflection of the disappearing spectral weight around the Fermi level. Fig. 7 shows the same Green's function in the Legendre representation [13]. Only the even Legendre coefficients are shown, since the odd coefficients vanish due to particle-hole symmetry. In this representation, the difference between $U = 2.42$ and $U = 2.46$ lies almost entirely on the first two coefficients. In that sense, the Legendre representation is not only mathematically efficient [13, 31] but also physically useful here: few coefficients are needed to describe the metal-insulator transition.

Figure 8 shows the symmetrized Jacobian, $X^{-1}JX$ at $U = 2.44$. All off-diagonal matrix elements are positive, whereas the diagonal elements become negative for larger Matsubara frequencies. The top-left matrix element is close to one. The leading eigenvector is heavily localized on the lowest Matsubara frequency, but necessarily has finite weight on the other frequencies as well, since the Jacobian matrix is not diagonal.

In Curie-Weiss mean-field theory, it is possible to find the critical point exactly (see Appendix B). This is relatively straightforward since the mean-field is a scalar in that case, and $h_c = 0$ is known from the symmetry of the system. In DMFT+IPT, the situation is more complicated, since the mean-field is dynamical and has

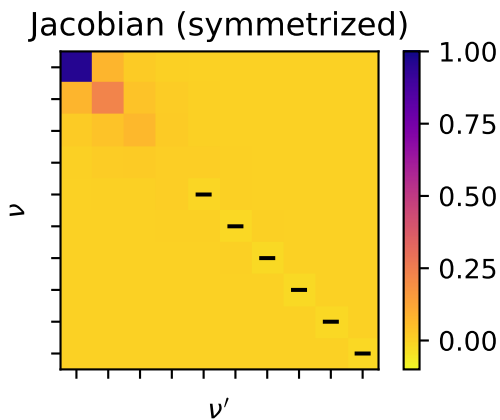


FIG. 8. Symmetrized Jacobian matrix at $U = 2.44$, $T = 1/20$. The lowest Matsubara frequencies are at the top/left. Negative matrix elements are indicated by a $-$ in the matrix. Only the top-left corner of the (infinite) matrix is shown, at high frequency the matrix is approximately diagonal, with a negative diagonal element that decays in magnitude.

infinitely many degrees of freedom. The Jacobian is expressed entirely in terms of t , U and G_0 . With a good Ansatz/parametrization for G_0 close to the critical point, it might be possible to derive further results about the critical parameters U_c and β_c , such as formal bounds on their values.

XII. CONCLUSION AND DISCUSSION

Via the susceptibility, a single DMFT calculation does not just provide information about a single point in the parameter space, but also about the immediate surroundings: the free energy landscape, the stability of solutions and the response to changing parameters. Here, this has been illustrated for the Bethe lattice. The Jacobian determines the stability of DMFT. Going from the non-interacting to the atomic limit, the eigenvalues of the Jacobian have to change sign. At the boundaries of the hysteresis region, in particular at the critical endpoint, the leading eigenvalue reaches unity. For the exact DMFT solution on the Bethe lattice, there is also a particularly simple relationship between the Jacobian and the Hessian of the free energy functional. However, unfortunately, the IPT approximation breaks some of the properties of the exact solution, and the Hessian derived in this way would be non-symmetric. Thus, DMFT+IPT cannot be written consistently in terms of a free energy functional. This shows one of the limitations of using an approximate impurity solver. The iterative stability of DMFT+IPT can still be analyzed based on the eigenvalues of the non-symmetric Jacobian matrix.

The Jacobian also appears in response functions such as $d\Sigma/dU$. As a result, it is possible to prove $d\Sigma(\tau)/dU < 0$ for any stable DMFT+IPT solution. Since the Jacobian appears in the denominator, Σ changes rapidly close

to the boundaries of the hysteresis region.

For the IPT approximation, the vertex has been derived explicitly. At particle-hole symmetry, the vertex depends on the input G_0 only via the combination $G_0 * G_0$. It can be written as the difference of a Toeplitz and a Hankel matrix, which both have a very simple frequency-dependence. This explicit expression could form the basis for further analytical considerations of, e.g., the critical point.

Efficient, alternative representations of the many-body Green's function have received considerable attention recently [13, 32, 33]. For an overview, see Ref. [34]. The motivation for these studies is the inefficiency of the Matsubara representation, i.e., the slow, algebraic decay of $G(i\nu_n)$ and $\Sigma(i\nu_n)$. For the finite temperature metal-insulator transition, the relevant physical information distinguishing between a metal and an insulator is largely concentrated at a small number low frequencies, supporting the idea that more compact representations are possible and useful. Indeed, few Legendre coefficients are sufficient to describe the physical changes close to the critical point. For future work, it would be interesting to perform some of the analysis of the vertex and the Jacobian directly in these alternative representations. Ideally, the representation used for the Green's function should closely match the eigenvectors of the Jacobian, since the magnitude of the eigenvalues of the Jacobian provides a useful criterion for physically relevant and irrelevant degrees of freedom. The Matsubara representation is in this sense efficient in the two trivial limits of the Hubbard model, $U \approx 0$ and $U \gg t$, since the Jacobian is frequency-diagonal in these two cases. Although it is not a compact representation per se, it is worth mentioning recent progress in fast solvers in the real time domain [35], potentially enabling accurate simulations of the spectral properties of the metal-insulator transition and the hysteresis region.

It is also noteworthy that the irreducible vertex of the impurity model was not needed in this discussion of the metal-insulator transition on the two-particle level, since all derivations were done with G_0 or Δ and not with G . Since it was not necessary to calculate the irreducible vertex via the inversion of a local Bethe-Salpeter equation, divergences that appear in this inversion procedure [36] are avoided completely in the present formalism.

The DMFT self-consistency conditions were solved using forward iteration here. Other, faster schemes have been used [12, 16], which are based on the iterative determination of the Jacobian. Since the explicit form of the DMFT Jacobian is given by Eq. (20), it might be used to initialize these faster self-consistency schemes. Apart from IPT, the vertex is generally not known and not cheap to calculate, but even an initial guess for the Jacobian based on an approximate version of the vertex could help speed up the convergence. Similar efficient mixing schemes have also been used in other electronic structure applications [37–39].

ACKNOWLEDGMENTS

The author would like to acknowledge useful discussions with Niklas Witt, Friedrich Krien, Emanuel Gull, Koen Reijnders and Hugo Strand. This work is supported by the Gyllenstierna Krapperrup's Foundation.

-
- [1] A. Georges, G. Kotliar, W. Krauth, and M. J. Rozenberg, Dynamical mean-field theory of strongly correlated fermion systems and the limit of infinite dimensions, *Rev. Mod. Phys.* **68**, 13 (1996).
- [2] A. Khurana, Electrical conductivity in the infinite-dimensional hubbard model, *Phys. Rev. Lett.* **64**, 1990 (1990).
- [3] G. Kotliar, E. Lange, and M. J. Rozenberg, Landau theory of the finite temperature Mott transition, *Phys. Rev. Lett.* **84**, 5180 (2000).
- [4] N. Blümer, *Mott-Hubbard Metal-Insulator Transition and Optical Conductivity in High Dimensions*, Ph.D. thesis, University of Augsburg (2002).
- [5] E. G. C. P. van Loon, F. Krien, and A. A. Katanin, Bethe-salpeter equation at the critical end point of the mott transition, *Phys. Rev. Lett.* **125**, 136402 (2020).
- [6] F. Krien, E. G. C. P. van Loon, M. I. Katsnelson, A. I. Lichtenstein, and M. Capone, Two-particle fermi liquid parameters at the mott transition: Vertex divergences, landau parameters, and incoherent response in dynamical mean-field theory, *Phys. Rev. B* **99**, 245128 (2019).
- [7] C. Melnick and G. Kotliar, Fermi-liquid theory and divergences of the two-particle irreducible vertex in the periodic anderson lattice, *Phys. Rev. B* **101**, 165105 (2020).
- [8] M. Reitner, P. Chalupa, L. Del Re, D. Springer, S. Ciuchi, G. Sangiovanni, and A. Toschi, Attractive effect of a strong electronic repulsion: The physics of vertex divergences, *Phys. Rev. Lett.* **125**, 196403 (2020).
- [9] G. Rohringer, A. Valli, and A. Toschi, Local electronic correlation at the two-particle level, *Phys. Rev. B* **86**, 125114 (2012).
- [10] H. Hafermann, K. R. Patton, and P. Werner, Improved estimators for the self-energy and vertex function in hybridization-expansion continuous-time quantum monte carlo simulations, *Phys. Rev. B* **85**, 205106 (2012).
- [11] J. B. Rigo and A. K. Mitchell, Automatic differentiable numerical renormalization group (2021), arXiv:2108.09575 [cond-mat.str-el].
- [12] H. U. R. Strand, A. Sabashvili, M. Granath, B. Hellsing, and S. Östlund, Dynamical mean field theory phase-space extension and critical properties of the finite temperature mott transition, *Phys. Rev. B* **83**, 205136 (2011).
- [13] L. Boehnke, H. Hafermann, M. Ferrero, F. Lechermann, and O. Parcollet, Orthogonal polynomial representation of imaginary-time green's functions, *Phys. Rev. B* **84**, 075145 (2011).
- [14] O. Parcollet, M. Ferrero, T. Ayrál, H. Hafermann, I. Krivenko, L. Messio, and P. Seth, Triqs: A toolbox for research on interacting quantum systems, *Computer Physics Communications* **196**, 398 (2015).
- [15] A. Georges, G. Kotliar, and Q. Si, Strongly correlated systems in infinite dimensions and their zero dimensional counterparts, *International Journal of Modern Physics B* **6**, 705 (1992).
- [16] R. Žitko, Convergence acceleration and stabilization of dynamical mean-field theory calculations, *Phys. Rev. B* **80**, 125125 (2009).
- [17] This related to the mathematical theorem called Poincaré's lemma. It is very similar to the statement that a vector field is curl-free if and only if it is the gradient of a scalar function, which is familiar from electromagnetism. That the Jacobian of the derivative of a scalar function is symmetric follows from Clairaut's theorem. If the Jacobian of f is symmetric, the function $g(x)$ can be defined as $g(x) = \int_{x_0}^x f(y) \cdot dy$ and the symmetry of the Jacobian of f guarantees that this integral is independent of the chosen path.
- [18] Note that $\Delta(i\nu)$ is purely imaginary, so the sign of $\delta^2\Omega/\delta(i\Delta)$ should be considered, which results in a minus sign.
- [19] M. Eckstein, M. Kollar, M. Potthoff, and D. Vollhardt, Phase separation in the particle-hole asymmetric hubbard model, *Phys. Rev. B* **75**, 125103 (2007).
- [20] To be more precise, $d\Sigma(\tau)/dU$ is the self-energy as a function of the imaginary time difference τ , where it is implied that the derivative with respect to U does not break time translation symmetry.
- [21] E. G. C. P. van Loon, Zenodo record: Two-particle correlations and the metal-insulator transition: Iterated Perturbation Theory revisited (2021).
- [22] D. Springer, P. Chalupa, S. Ciuchi, G. Sangiovanni, and A. Toschi, Interplay between local response and vertex divergences in many-fermion systems with on-site attraction, *Phys. Rev. B* **101**, 155148 (2020).
- [23] A related question is if the G_0 is physical, in the sense that it is the Laplace transform of a positive semi-definite density of states, and if the functional derivative can be constrained to the manifold of physical Green's functions. Since the IPT expression for the self-energy is written entirely in imaginary time, however, this question is not our concern here.
- [24] Note that this generally holds for a susceptibility defined in imaginary time as $\chi(\tau) = G(\tau)G(\tau)$. This is the usual expression for the particle-particle susceptibility. Due to particle-hole symmetry, it holds for the particle-hole susceptibility as well here.
- [25] Further mathematical progress could be made under the assumption that $G_0(\tau)$ is causal, in the sense that it originates from a positive density of states. One way is to use the Lehmann representation of G_0 to derive a Lindhard formula for $G_0 * G_0$. Alternatively, it implies that $\partial_\tau^{2n} G_0(\tau)$ is sign-definite for any n .
- [26] P. Thunström, O. Gunnarsson, S. Ciuchi, and

- G. Rohringer, Analytical investigation of singularities in two-particle irreducible vertex functions of the hubbard atom, *Phys. Rev. B* **98**, 235107 (2018).
- [27] E. W. Weisstein, Gershgorin circle theorem, <https://mathworld.wolfram.com/GershgorinCircleTheorem.html>.
- [28] F. Krien, A. Valli, and M. Capone, Single-boson exchange decomposition of the vertex function, *Phys. Rev. B* **100**, 155149 (2019).
- [29] N. Wentzell, G. Li, A. Tagliavini, C. Taranto, G. Rohringer, K. Held, A. Toschi, and S. Andergassen, High-frequency asymptotics of the vertex function: Diagrammatic parametrization and algorithmic implementation, *Phys. Rev. B* **102**, 085106 (2020).
- [30] Note that, although $\Sigma^{\text{IPT}} = \Sigma^{\text{Exact}}$ at $t = 0$, this does not imply that the corresponding vertices are also equal, so the proportionality of the vertex with the identity matrix is a result that is derived within the IPT approximation. For a detailed investigation of the atomic limit, see Ref. [26].
- [31] X. Dong, D. Zgid, E. Gull, and H. U. R. Strand, Legendre-spectral dyson equation solver with super-exponential convergence, *The Journal of Chemical Physics* **152**, 134107 (2020), <https://doi.org/10.1063/5.0003145>.
- [32] H. Shinaoka, J. Otsuki, M. Ohzeki, and K. Yoshimi, Compressing green's function using intermediate representation between imaginary-time and real-frequency domains, *Phys. Rev. B* **96**, 035147 (2017).
- [33] J. Li, M. Wallerberger, N. Chikano, C.-N. Yeh, E. Gull, and H. Shinaoka, Sparse sampling approach to efficient ab initio calculations at finite temperature, *Phys. Rev. B* **101**, 035144 (2020).
- [34] H. Shinaoka, N. Chikano, E. Gull, J. Li, T. Nomoto, J. Otsuki, M. Wallerberger, T. Wang, and K. Yoshimi, Efficient ab initio many-body calculations based on sparse modeling of matsubara green's function (2021), [arXiv:2106.12685](https://arxiv.org/abs/2106.12685) [cond-mat.str-el].
- [35] J. Kaye and H. U. R. Strand, A fast time domain solver for the equilibrium dyson equation (2021), [arXiv:2110.06120](https://arxiv.org/abs/2110.06120) [math.NA].
- [36] P. Chalupa, P. Gunacker, T. Schäfer, K. Held, and A. Toschi, Divergences of the irreducible vertex functions in correlated metallic systems: Insights from the anderson impurity model, *Phys. Rev. B* **97**, 245136 (2018).
- [37] P. Pulay, Convergence acceleration of iterative sequences. the case of scf iteration, *Chemical Physics Letters* **73**, 393 (1980).
- [38] J. Kaufmann, C. Eckhardt, M. Pickem, M. Kitatani, A. Kauch, and K. Held, Self-consistent ladder dynamical vertex approximation, *Phys. Rev. B* **103**, 035120 (2021).
- [39] F. Krien, P. Worm, P. Chalupa, A. Toschi, and K. Held, Spin scattering turns complex at strong coupling: the key to pseudogap and fermi arcs in the hubbard model (2021), [arXiv:2107.06529](https://arxiv.org/abs/2107.06529) [cond-mat.str-el].
- [40] D. Hügel, P. Werner, L. Pollet, and H. U. R. Strand, Bosonic self-energy functional theory, *Phys. Rev. B* **94**, 195119 (2016).
- [41] G. Rohringer and A. Toschi, Impact of nonlocal correlations over different energy scales: A dynamical vertex approximation study, *Phys. Rev. B* **94**, 125144 (2016).

Appendix A: Asymptotic expressions

Here, a brief overview is given of some known properties of many-body Green's functions at large frequencies. More rigorous mathematical treatment can be found elsewhere in the literature [40, 41].

The Matsubara functions $G(i\nu_n)$, $G_0(i\nu_n)$ and $\Sigma(i\nu_n)$ decay algebraically at large frequency, e.g.,

$$G(i\nu_n) \xrightarrow{\nu_n \rightarrow \infty} G(M=0) + \frac{G(M=1)}{(i\nu_n)} + \frac{G(M=2)}{(i\nu_n)^{-2}} + \dots, \quad (\text{A1})$$

where the coefficients $G(M)$ are called the tail coefficients of G . At particle-hole symmetry, $\text{Re } G(i\nu_n) = 0$, so all even tail coefficients vanish and the lowest-order relevant coefficients are $G(M=1)$ and $G(M=3)$. These coefficients are related to the moments of the (real-energy) spectral function, for example $G(M=1)$ gives the integral of the spectral function and $G(M=3)$ gives its second moment.

In the imaginary time representation, the first tail coefficient is responsible for the discontinuity at $\tau = 0$,

$$\begin{aligned} G(M=1) &= \lim_{n \rightarrow \infty} i\nu_n G(i\nu_n) \\ &= \lim_{n \rightarrow \infty} i\nu_n \int_0^\beta d\tau G(\tau) e^{i\nu_n \tau} \\ &= \lim_{n \rightarrow \infty} \int_0^\beta d\tau G(\tau) \frac{d}{d\tau} e^{i\nu_n \tau} \\ &= G(\tau) e^{i\nu_n \tau} \Big|_{0^+}^{\beta^-} - \lim_{n \rightarrow \infty} \int_0^\beta d\tau \frac{dG(\tau)}{d\tau} e^{i\nu_n \tau} \\ &= -1 \cdot G(\tau = \beta^-) - G(\tau = 0^+) \\ &= G(\tau = 0^-) - G(\tau = 0^+) \end{aligned} \quad (\text{A2})$$

Here, $e^{i\nu_n \beta} = -1$ was used and it is argued that the second term in the integration by parts vanishes in the limit of large frequency, since $dG/d\tau$ is smooth on $(0, \beta)$.

Similarly, the third coefficient is related to the discontinuity in the second derivative of $G(\tau)$ at $\tau = 0$, and so on. This can be proven via integration by parts, similar to the proof above. The vanishing of the even coefficients in the particle-hole symmetric system is equivalent to the continuity of the odd derivatives of $G(\tau)$ at $\tau = 0$.

From the DMFT-IPT relations, it is possible to derive some of the lowest-order tail coefficients exactly. The self-consistency equation $G_0 = 1/(i\nu_n - t^2 G)$ implies $G_0(M=1) = 1$ and $G_0(M=3) = t^2 G(M=1)$ for the self-consistent solution. Dyson's equation $G = G_0/(1 - \Sigma G_0)$ implies $G(M=1) = G_0(M=1)$ and $G(M=3) = G_0(M=3) + G_0(M=1)\Sigma(M=1)G_0(M=1)$. Finally, the first moment of Σ in IPT is most easily derived in imaginary time, since $G_0(M=1)$ combined with particle-hole symmetry leads to $G_0(\tau = 0^-) = 1/2$ and

$$G_0(\tau = 0^+) = -1/2$$

$$\Sigma^{\text{IPT}}(M = 1) = \Sigma(\tau = 0^-) - \Sigma(\tau = 0^+) \quad (\text{A3})$$

$$= U^2 [G_0(\tau = 0^-)^3 - G_0(\tau = 0^+)^3] \quad (\text{A4})$$

$$= \frac{U^2}{4}. \quad (\text{A5})$$

Note that the latter relation also holds for the exact self-energy at particle-hole symmetry, not just for the IPT approximation. Collecting the results,

$$G_0(i\nu_n) \xrightarrow{\nu_n \rightarrow \infty} \frac{1}{i\nu_n} + \frac{t^2}{(i\nu_n)^3} + \dots \quad (\text{A6})$$

$$G(i\nu_n) \xrightarrow{\nu_n \rightarrow \infty} \frac{1}{i\nu_n} + \frac{t^2 + U^2/4}{(i\nu_n)^3} + \dots \quad (\text{A7})$$

$$\Sigma(i\nu_n) \xrightarrow{\nu_n \rightarrow \infty} \frac{U^2}{4} \frac{1}{i\nu_n} + \dots, \quad (\text{A8})$$

shows that the first few tail coefficients can be expressed entirely in terms of the *parameters* t and U . This has the important implication that any co-existing solutions in the hysteresis region have the same asymptotic coefficients and therefore differ only “at small frequencies”, in the sense that $\Sigma^{\text{metal}} - \Sigma^{\text{insulator}}$ decays at least as $(i\nu_n)^{-3}$ and $G_0^{\text{metal}} - G_0^{\text{insulator}}$ decays at least as $(i\nu_n)^{-5}$.

On the other hand, the third moment of the self-energy,

$$\begin{aligned} \Sigma^{\text{IPT}}(M = 3) &= \left. \frac{d^2 \Sigma(\tau)}{d\tau^2} \right|_{0^+}^{0^-} \quad (\text{A9}) \\ &= \left(3U^2 G_0^2 \frac{d^2 G_0(\tau)}{d\tau^2} + 6U^2 G_0 \left(\frac{dG}{d\tau} \right)^2 \right) \Big|_{0^+}^{0^-} \\ &= \frac{3U^2}{4} G_0(M = 3) + 6U^2 \left(\frac{dG_0}{d\tau} \Big|_{\tau=0} \right)^2. \end{aligned}$$

Here, the actual value of the first derivative of $G(\tau)$ at $\tau = 0$ enters, not just the discontinuity. Thus, the right-hand side of this expression cannot be expressed entirely in terms of the parameters and can be different for co-existing solutions of the self-consistency relation. All results in this Appendix also hold for the exact DMFT solution on the particle-hole symmetric Bethe lattice.

Appendix B: Curie-Weiss mean-field theory

Curie-Weiss mean-field theory for the spin-1/2 Ising model is perhaps the most familiar example of a mean-field theory. Reducing the notation to a minimum, it is defined by the set of equations

$$M(h) = \tanh(\beta h), \quad (\text{B1})$$

$$h = B + \alpha M. \quad (\text{B2})$$

Here, $M(h)$ is the magnetization of the impurity model as a function of the self-consistent field h and $h = B + \alpha M$ is

the self-consistency relation. The physical variables are the inverse temperature β and the external field strength B , α is a fixed constant. Clearly $h = 0$ and $M = 0$ is always a solution when $B = 0$.

The stability of this solution is given by the “Jacobian”, $J = dM^{\text{new}}/dM^{\text{old}} = dM/dh \cdot \partial h/\partial M = \alpha dM/dh = \alpha\beta/\cosh^2(\beta h)$. Filling in $h = 0$ gives $J = 1$ if and only if $\alpha\beta = 1$. In other words, $\beta_c = 1/\alpha$.

The physical susceptibility dM/dB can be written as

$$\frac{dM}{dB} = \frac{dM}{dh} \frac{dh}{dB} = \frac{dM}{dh} \left(1 + \alpha \frac{dM}{dB} \right) \quad (\text{B3})$$

$$\frac{dM}{dB} = \frac{dM/dh}{1 - \alpha dM/dh}. \quad (\text{B4})$$

This diverges at the critical point $J = 1$, since the denominator is equal to zero there. This illustrates the relation between the Jacobian and the response function in Curie-Weiss mean-field theory.

Appendix C: Representations of the vertex

In the main text, the reducible vertex of IPT is derived both in imaginary time and in imaginary frequency. To see how these two expressions are related, it is useful to derive the imaginary time result in a slightly more general set-up. In the main text, time translation symmetry is assumed throughout the derivation and Σ and G are written as a function of a single imaginary time argument. This implicitly sets the bosonic frequency ω of the vertex to zero.

Instead, it is also possible to start from the two-time expression

$$\Sigma^{\text{IPT}}(\tau_1, \tau_2) = -U^2 G_0(\tau_1, \tau_2) G_0(\tau_2, \tau_1) G_0(\tau_1, \tau_2). \quad (\text{C1})$$

For the vertex, this gives a four-time object

$$\begin{aligned} \frac{\partial \Sigma(\tau_1, \tau_2)}{\partial G_0(\tau_3, \tau_4)} &= -2U^2 \delta_{\tau_1, \tau_3} \delta_{\tau_2, \tau_4} G_0(\tau_1, \tau_2) G_0(\tau_2, \tau_1) \\ &\quad - U \delta_{\tau_2, \tau_3} \delta_{\tau_1, \tau_4} G_0(\tau_1, \tau_2) G_0(\tau_1, \tau_2). \quad (\text{C2}) \end{aligned}$$

Now, when considering variations around the time translation symmetric solution, time translation symmetry can be used on the right-hand side, i.e., $G_0(\tau_1, \tau_2) = G_0(\tau_2 - \tau_1)$. Particle-hole symmetry gives $G_0(\tau) = -G_0(-\tau)$. Together, this leads to

$$\begin{aligned} \frac{\partial \Sigma(\tau_1, \tau_2)}{\partial G_0(\tau_3, \tau_4)} &= 2U^2 \delta_{\tau_1, \tau_3} \delta_{\tau_2, \tau_4} G_0^2(\tau_2 - \tau_1) \\ &\quad - U \delta_{\tau_2, \tau_3} \delta_{\tau_1, \tau_4} G_0^2(\tau_2 - \tau_1). \quad (\text{C3}) \end{aligned}$$

Clearly, every part of this formula only depends on time differences. The appearance of two δ functions means that both terms depend on a single linear combination of frequencies only. This is reflected in the appearance of $\chi(i\nu - i\nu')$ and $\chi(i\nu + i\nu')$ in the main text.

Appendix D: Zero temperature

The main text studies the IPT solution of the Bethe lattice Hubbard model at finite temperature. The limits of small and large interaction provided insight in the structure of the theory, especially on the two-particle level. Here, the limit $T \rightarrow 0$ is considered, where some additional analytical results can be derived both in the limit of small U and large U .

1. Atomic limit

For the insulating side, the atomic limit is a useful starting point. In particular, it has $G_0(i\nu) = 1/i\nu$, $\Sigma(i\nu) = U^2/(4i\nu)$ and $\chi(i\omega_m) = \frac{1}{4T^2}\delta_{m,0}$. This gives $G^{-1}(i\nu_0) = G_0^{-1}(i\nu_0) - \Sigma(i\nu_0) \approx -\Sigma(i\nu_0)$. The leading eigenvalue of the Jacobian is determined by the diagonal matrix element of the vertex contribution, $\lambda \approx J^\Sigma(\nu_0, \nu_0)$,

$$\begin{aligned} \lambda &\approx \frac{3U^2t^2}{\beta^2} G_0^2(i\nu_0) G^2(i\nu_0) \chi(\omega_0) \\ &\approx \frac{3U^2t^2}{\beta^2} \frac{1}{\pi^2 T^2} \frac{16\pi^2 T^2}{U^4} \frac{1}{4T^2} \\ &= \frac{12t^2}{U^2} \text{ for large } U. \end{aligned} \quad (\text{D1})$$

2. Non-interacting limit

The limit $T \rightarrow 0$ implies that the discrete Matsubara frequencies approach the origin of the complex plane, so $G_0(i\nu)$ is directly related to $G_0(E=0)$ in this limit. At

small U , G_0 stays close to the non-interacting value, at least in the sense that $\text{Im} G_0(i\nu) \rightarrow -\frac{1}{t}$ for $\nu \approx 0^+$. For the IPT vertex, the difference of two susceptibilities is needed. The simplest case is

$$\chi(i\omega_0) - \chi(i\omega_1) = \sum_m G(i\nu_m) [G(i\nu_m) - G(i\nu_{m-1})] \quad (\text{D2})$$

$$\begin{aligned} &\approx G(i\nu_0) [G(i\nu_0) - G(i\nu_{-1})] \\ &+ \sum_{m \neq 0} G(i\nu_m) 2\pi T \frac{dG(i\nu)}{d(i\nu)} \end{aligned} \quad (\text{D3})$$

$$= 2G(i\nu_0)^2 + O(T) \quad (\text{D4})$$

$$= 2t^{-2} \text{ for } T \rightarrow 0. \quad (\text{D5})$$

Here, it was used that at low temperature, the Matsubara grid becomes dense and $G(i\nu_n)$ is a smooth function except between ν_{-1} and ν_0 , where it jumps from $+1/t$ to $-1/t$. A similar derivation shows that $\chi(i\omega_m) - \chi(i\omega_{m'}) = (m' - m) \cdot 2t^{-2}$ for $m' > m \geq 0$. The structure of Fig. 2 means that the first row and column of the vertex are constant and equal to $3\frac{U^2}{\beta^2} 2t^{-2}$, the second row and column are constant and equal to $3\frac{U^2}{\beta^2} \cdot 3 \cdot 2t^{-2}$ except for their first elements, and so on. The factor in front of the vertex $\beta^{-2} = T^2$ makes the low-frequency components of the vertex disappear in the limit $T \rightarrow 0$. Since $G_0(i\nu_0)$ is approximately constant in the limit of low temperature, the vertex contribution J^Σ in Eq. (20) indeed vanishes compared to J^0 , and the leading eigenvalue is still given by $t^2 G^2(i\nu_0)$, with the eigenvector concentrated on the lowest Matsubara frequency. So at small U , the result is $\lambda_J \approx -1$.